Experimental characterization and validation by FEM analyses of a 3D-printed support

Experimental characterization and validation by FEM analyses of a 3D-printed support

F Cosmi[1] **and A Dal Maso**[1]

[1] University of Trieste, Department of Engineering and Architecture, Via Valerio 1, Trieste, Italy.
Corresponding author: cosmi@units.it

Abstract. Devices for training of healthcare specialists are widespread applications of 3D printing. BES TEST™ is an innovative test for the diagnosis of osteoporosis and similar bone diseases, based on mechanical simulations performed on a virtual biopsy of the patient's fingers, obtained by radiograms. Operator training is performed on a phantom hand, which is held in place by a specifically-designed support, which was 3D printed using stereolithography (SLA) with Formlabs Tough V5™ resin. Our aim is twofold: (1) perform a mechanical characterization of the resin and (2) verify that the obtained material characteristics can be used for the design of 3D-printed parts, in particular the phantom hand support. Tensile tests were performed following ISO-527. FEM analyses were carried out on the support CAD model adopting the experimentally-obtained material properties. The calculated displacements were compared with those measured experimentally on the prototype, which was manufactured using the same 3D printing and post-curing parameters as the tensile samples. FEM and experimental results were in very good agreement (error < 5.5%): this confirms that, when studying the mechanical performance of SLA 3D-printed parts, it is good practice to characterize the resin using the same printing and post-curing parameters as the final part.

1. Introduction

The applications of Additive Manufacturing (AM) in the healthcare industry are many and fast-growing. 3D-printed protheses and similar medical devices are currently being employed in orthopedics [1,2]; nanoscale drug-delivery systems can be rapidly designed and tailored for each specific patient's needs [3]; 3D-printed aligners are becoming the norm among dentists [4]. These are just some examples, but one of the most widespread applications of AM in medicine is the creation of educational models for the training of surgeons and technicians [5-10].

BES TEST™ is a recently-developed diagnostic exam for osteoporosis and similar bone diseases, based on mechanical simulations performed on a virtual biopsy of the patient's hand bones [11,12]. Three plain radiographic images of the proximal epiphysis of the first phalanges of the patient's non-dominant hand are required for each analysis. These images are acquired with a handheld x-ray device coupled with a sensor, thus minimizing the radiation dose to the patient. Some skill and practice are necessary for the operator to locate these bones and to position the x-ray device correctly, so as to obtain properly-centered radiograms: training is achieved with the help of a phantom hand.

In clinical practice, patients are required to hold their hand open and still during the radiographic acquisitions, approximately 15 cm above a table (or an equivalent horizontal surface where the elbow can rest). In order to ease and to standardize the process, a specific ergonomic support was designed and successfully tested [13]. However, the same support cannot be used for a phantom hand, since it is

impractical to fasten the phantom hand to it and to hold it in balance. Therefore, a different support was designed for training purpose and was 3D-printed using stereolithography (SLA).

In SLA, a part is created layer after layer by selectively curing a photopolymerizing liquid resin with a controlled laser beam [14]. In desktop SLA 3D printers, parts are generated upside down and dipped in the liquid resin only for the last few layers: this limits the amount of extra resin that is required for the process.

The principal advantages of Stereolithography over low-budget 3D-printing technologies (i.e. Fused Deposition Modelling) are:

- greater overall dimensional accuracy [15,16];
- better surface finish [17-19];
- possibility of creating watertight parts [20];
- near-isotropic material behavior [21-26];
- higher printing speed;
- user-friendliness.

At the end of each print, it is recommended to post-cure the generated parts, to confer better mechanical properties to the material [27]. Post-curing consists of simultaneously:

- heating the part to a determined temperature;
- exposing the part to UV radiations.

Post-curing helps obtain completely crosslinked photopolymer chains, thus strengthening the chemical bonds within the material [28]. This increases strength, stiffness and temperature resistance. Each specific material has its optimal post-cure settings, which are usually provided by the manufacturer, together with the material characteristics of both the uncured and the cured resin. However, it is extremely difficult to guarantee a uniform heat distribution within the cured part. Moreover, it is virtually impossible to irradiate every surface of a perhaps complex model with the same amount of UV light: concave models or bulky parts particularly suffer the problem, as there is no way for the UV rays to reach the innermost volumes. Therefore, the manufacturer's stated mechanical properties might differ noticeably from those measured in practice on the actual load-bearing part.

In literature, there are several studies that attempt to optimize the printing parameters of AM in relation to the desired mechanical properties. However, most of these tend to focus on FDM rather than SLA, for which little work has been published [29,30]. Moreover, most are based solely on empirical data or on numerical simulations. An exception to this is the paper by Yang et al. [31], where a mathematical model is proposed to predict the tensile strength and hardness of 3D-printed parts by calculating the local solidification level of the SLA resin. The authors claim that their model has been successfully validated through experimental measurements, but this validation has been performed – as in most other cases – on standard specimens, rather than on actual parts. Standard specimens have an extremely simple geometry, which is far from that of most 3D-printed parts, which exploit the geometrical versatility of AM. Therefore, it might be useful to measure the actual response to loads of end-use parts fabricated by AM and compare their predicted behavior to experimental results.

The aim of this work is twofold:

- to perform a mechanical characterization by tensile tests on standard specimens of the 3D-printed material used for the phantom hand support;
- to measure the displacement of the 3D-printed phantom hand support under its nominal loads and compare it to the predicted displacements, obtained through FEM simulations.

2. Materials and methods

2.1. Tensile testing setup

The specimens were manufactured by a Formlabs™ Form2™ SLA 3D printer using Tough V5™ resin and post-cured in the Form Cure™ oven. The adopted printing and post-curing parameters are reported in Table 1.

The specimens are of type 1BA, as suggested by the ISO-527 norm [32]. Figure 1 (a) shows the geometry of the specimens used.

Table 1. Printing and post-curing parameters.

Material	Layer height	Post-cure		
		Time	Irradiation	Temp.
Formlabs™ Tough V5™	50 µm	60 min	405 nm 9.1 W	60°C

The samples were printed at different angles on the buildplate to validate the isotropy obtained from the material and printing process. The printing angle θ is defined as the angle between the specimen's axis and the building direction (z axis), as shown in Figure 1 (b). The specimens were printed in vertical (0°), horizontal (90°) and at intermediate angles, with 15° intervals, for a total of 7 different orientations. To obtain greater statistical reliability, 3 specimens were printed per orientation, for a total of 21 printed samples.

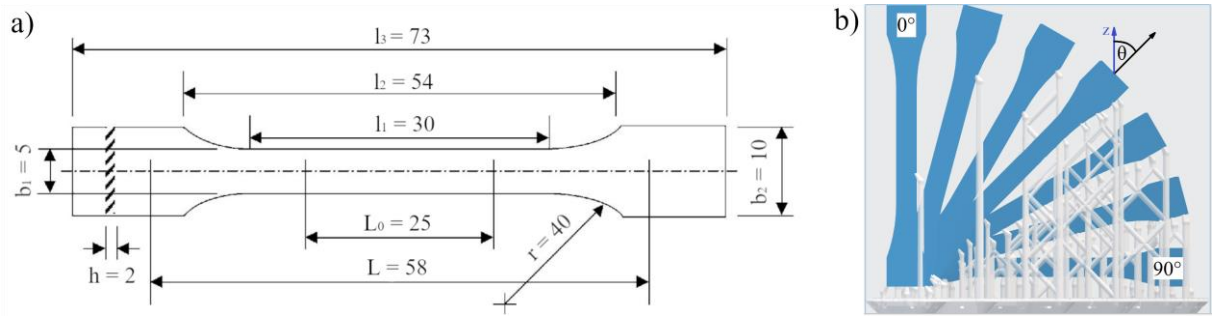

Figure 1. (a) ISO 527 Type 1BA specimen geometry. (b) Different orientations on buildplate.

The tensile tests were carried out on an in-house designed testing machine for low-budget applications, which had already been validated in previous studies [26,33]. These tests were performed in compliance with the ISO 527 guidelines [32]. Ambient temperature was 21 ± 1ºC.

2.2. Support design

The phantom hand (3M Diagnostic Imaging Products™, item code 34-7002-0826-6) is held in the same position a real patient would hold his/her hand during the test (i.e. open hand, thumb pointing upwards); there should be no obstacles on either side, as this would disrupt the radiographical acquisitions. The support includes a joint so that the phantom hand can be easily attached and removed: the phantom hand is already equipped with a 3D-printed male connector on its wrist. The support structure should be self-standing and properly balanced, both with and without the mounted phantom hand, light and sufficiently robust to withstand the weight of the phantom hand and any accidental stress during transport and use. Thanks to the extreme versatility of AM, there are very few constraints on the geometry – therefore the manufacturability – of the part.

The support was designed using SolidWorks™ and its CAD is shown in Figure 2 (a). The support was SLA 3D-printed (Figure 2 (b)) with the same resin and settings used for the specimens, previously described in Table 1.

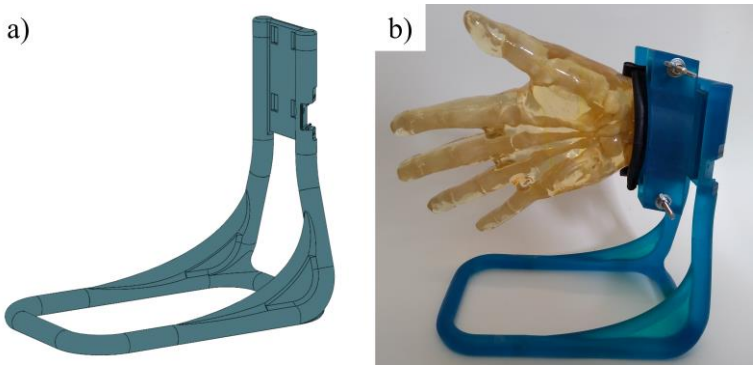

Figure 2. (a) CAD of the designed phantom hand support. (b) 3D-printed support with phantom hand.

2.3. FEM simulation setup

Linear FEM analyses were performed on the 3D model of the support using SolidWorks Simulation™. The experimentally obtained properties of the resin (see section 3.1) were used for the simulations. Two different loading configurations (I and II respectively) were investigated; in both cases the support base was fixed.

Configuration I. A vertical force F_y = 20 N was applied at l_f = 100 mm from the contact face between the phantom hand and the support. The y-displacement (d_y) was measured at l_m = 195 mm from the contact face (Figure 3 (a)). This represents the nominal loading configuration, where F_y is the weight of the phantom hand and l_f is the distance between the contact face and the hand's barycenter.

Configuration II. A horizontal force F_x = 20 N was applied at l_f = 195 mm from the contact face, horizontal displacement (d_x) was measured at l_m = 174 mm (Figure 3 (b)). This loading configuration represents a torsion that might occur from an improper use of the device or from an accidental fall to the ground.

To aid the definition of loads in the simulations, a thick rectangular beam was added to the CAD model: this makes it possible to apply forces and read the corresponding displacements at the desired positions without the need of calculating torques or applying other indirect measurement methods. The section of the beam is much greater than any part of the structure; a preliminary FEM analysis was conducted on just the auxiliary beam and it was found that its own deformations are less than two orders of magnitude smaller compared to the measured deformations. Therefore, under the applied loads, the beam results so stiff that it can be considered rigid.

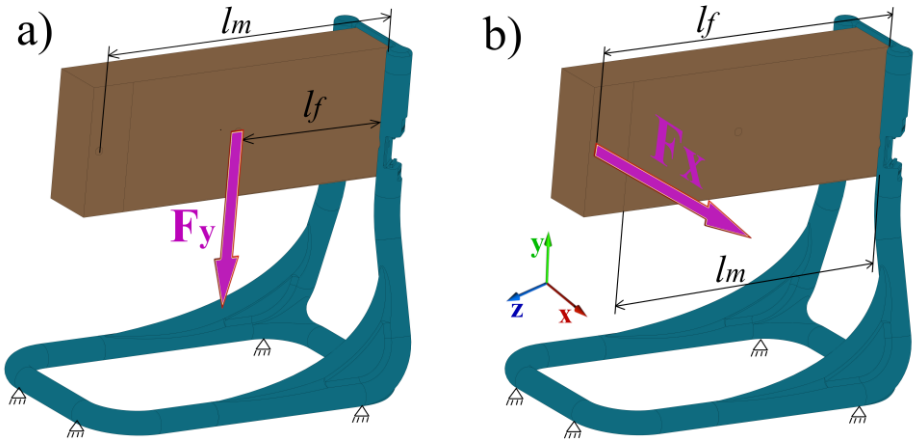

Figure 3. FEM simulation setup. (a) Configuration I; (b) Configuration II.

The generated meshes were curvature-based meshes, i.e. the size of the elements is defined locally by the curvature of the geometry. This option in SolidWorks Simulation™ is very helpful, since regions with greater curvature often correspond to the regions of greater stress. Mesh convergence was obtained with the h-adaptive method. The built-in h-adaptive method for mesh refinement decreases the average element size in the regions where the stresses calculated at the previous iteration are greater [34]. Convergence is reached when the change in strain energy between the previous and the present iteration is less than a determined value ε. For these simulations, this value was set to ε = 1%.

2.4. Experimental setup

The applied forces, the constraints and the positions for the displacement measurement depend on the specific configuration (I or II) and correspond to those previously described for the FEM analyses in section 2.3. As for the simulations, a rigid rectangular beam was fixed to the contact face to facilitate the application of loads and the displacement readings. The applied forces were obtained with a weight and, when necessary, a pulley system. The displacement was measured with a manual caliper (0.05 mm resolution). The ambient temperature during these tests was 21 ± 1ºC, the same adopted for the tensile tests. A schematic representation of the experimental setup for both configurations is shown in Figure 4.

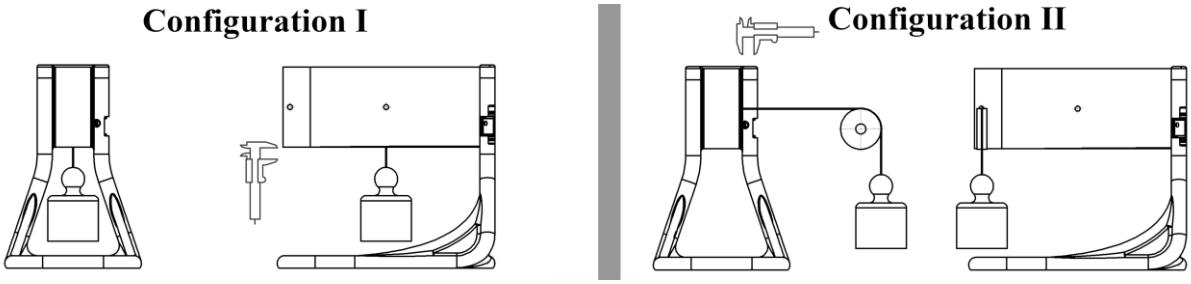

Figure 4. Experimental setup for Configuration I (left) and Configuration II (right).

Different values were assigned to F_x and F_y to verify the linear relationship between force and displacement: F_x and F_y ranged from 2.5 to 20 N with 2.5 N intervals, a total of 8 *levels*. The displacements d at l_m were measured five times with repositioning; the mean value ($\bar{d}$) and the standard deviation (SD) were calculated on the repeated measurements. The regression line of the average displacements within each level was computed; R^2 was calculated to quantify the goodness of fit.

3. Results

3.1. Tensile test results

The results of the tensile tests are presented in Figure 5, where tensile strength (or maximum stress) and Young's modulus are plotted as a function of the printing angle. The Kolmogorov-Smirnov (limiting form) normality test was performed: the resulting p-values (p = 0.52 for maximum stress, p = 0.96 for Young's modulus) suggest that in both cases the distribution is normal, therefore the fluctuations in maximum stress and modulus can be due to random errors. Since there is no evident relationship between θ and the mechanical characteristics of SLA 3D-printed Tough V5™ resin, this material can be considered isotropic.

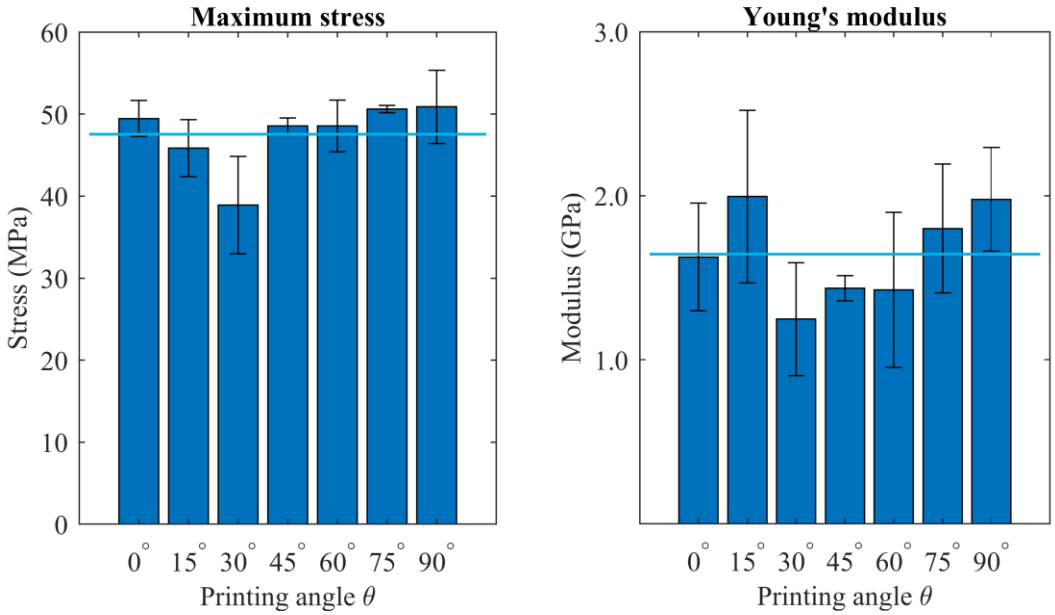

Figure 5. Tensile test results: maximum stress and Young's modulus. Error bars: ±SD. Horizontal line: overall mean.

Table 2 shows the overall mean material characteristics of the tested 3D-printed resin compared to those stated by the manufacturer [35].

Table 2. Mechanical characteristics of Formlabs Tough V5™ resin.

	Experimental	Datasheet
Maximum stress	47.5 ± 4.1 MPa	55.7 MPa
Young's modulus	1.64 ± 0.29 GPa	2.7 GPa

3.2. FEM simulation results

The results of the FEM analyses are reported shown in Figure 6. The deformed model is colored based on vertical displacement for configuration I and horizontal displacement for configuration II. The position at which the displacement was measured (l_m) is also reported.

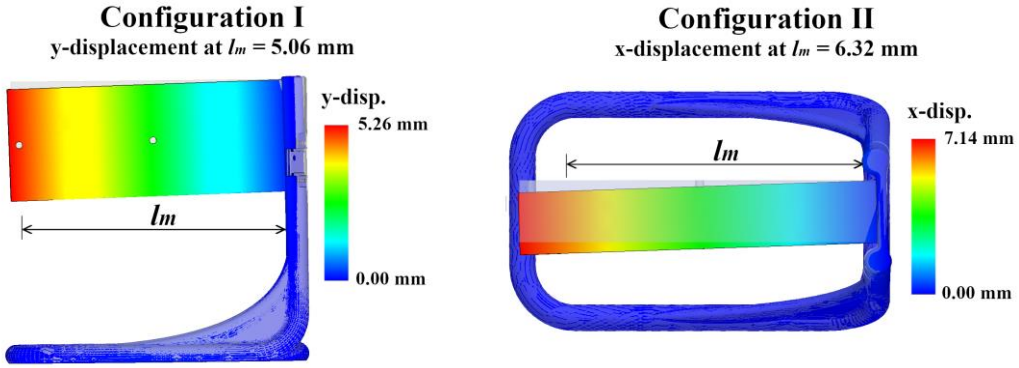

Figure 6. FEM results: displacement plots and graphical representation.

Figure 7 shows the meshed models: the elements are denser where the stress is greater. Mesh convergence plots are reported in Figure 8.

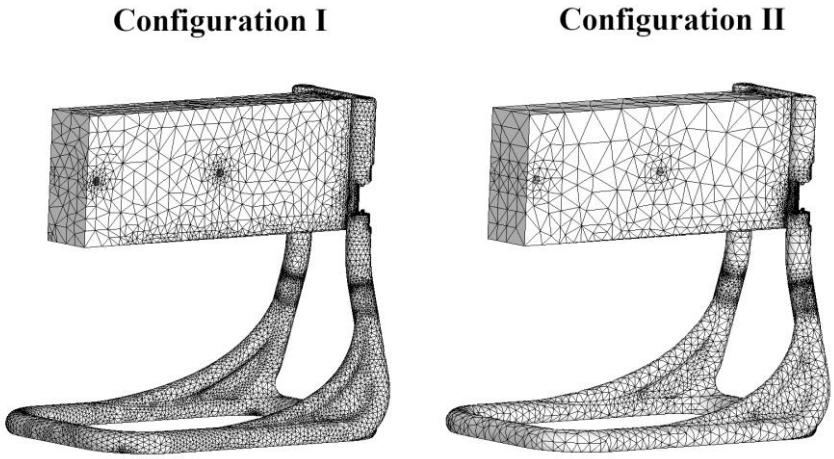

Figure 7. 3D representation of the final h-adapted meshes.

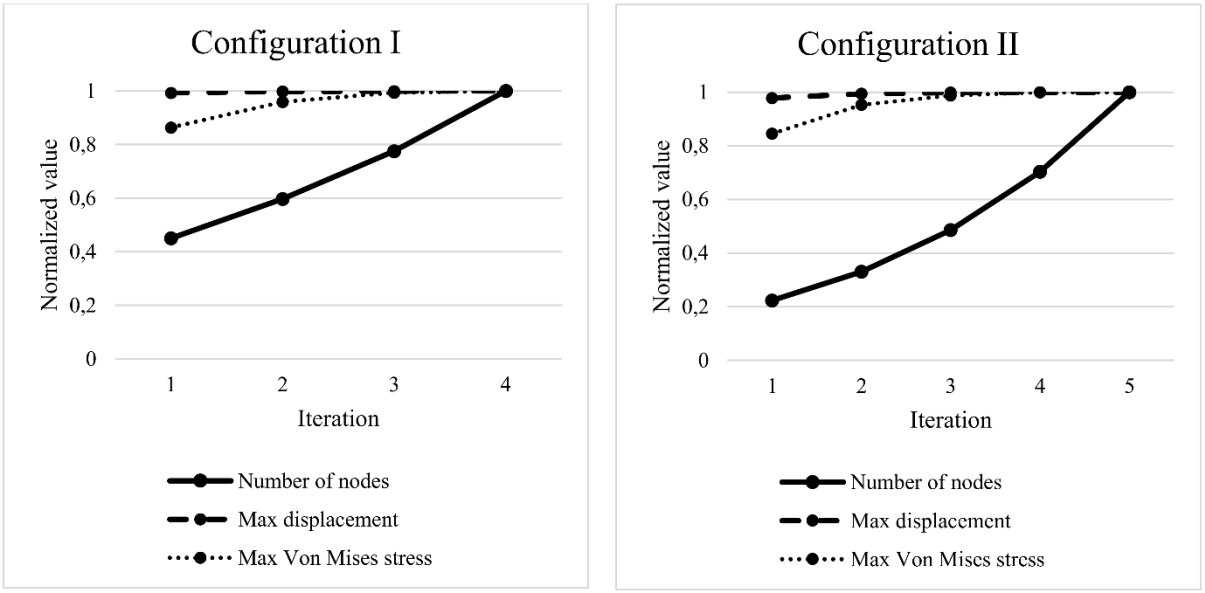

Figure 8. Mesh convergence plots. Normalized values referring to the final mesh.

Table 3 summarizes the principal simulation results and the main characteristics of the FEM mesh.

Table 3. FEM simulation results and final mesh characteristics.

	Configuration I	**Configuration II**
Applied force	F_y = 20 N	F_x = 20 N
Displacement at l_m	d_y = 5.06 mm	d_x = 6.32 mm
Type of mesh elements	Tetrahedral	Tetrahedral
Strain energy convergence threshold	Δ = 1%	Δ = 1%
Number of iterations to reach convergence	4	5
Final mesh number of nodes	5.17×10^5	3.59×10^5
Final mesh number of elements	3.43×10^5	2.35×10^5
Final mesh maximum element size	9.21 mm	18.58 mm
Final mesh minimum element size	1.84 mm	3.72 mm
Final mesh maximum element aspect ratio	216	224
Final mesh elements with aspect ratio > 10	1.27×10^3 (0.37%)	6.08×10^3 (2.59%)

3.3. Experimental validation

The force-displacement plot of the experimental measurements is shown in Figure 9. The mean and standard deviation at each level are represented by error bars. The regression line of the experimental data is represented by a dotted line. The R^2 values are reported for each configuration and are very close to 1, therefore the experimental relationship between force and displacement can be considered linear with good approximation. In the FEM simulations, the force-displacement plot is linear by definition and is reported in Figure 9 for comparison. The error between the experimental and simulation results can be defined as:

$$\epsilon = \frac{|Exp - FEM|}{Exp}$$

where *Exp* and *FEM* are the slopes of the experimental (regression) and numerical force-displacement lines, respectively.

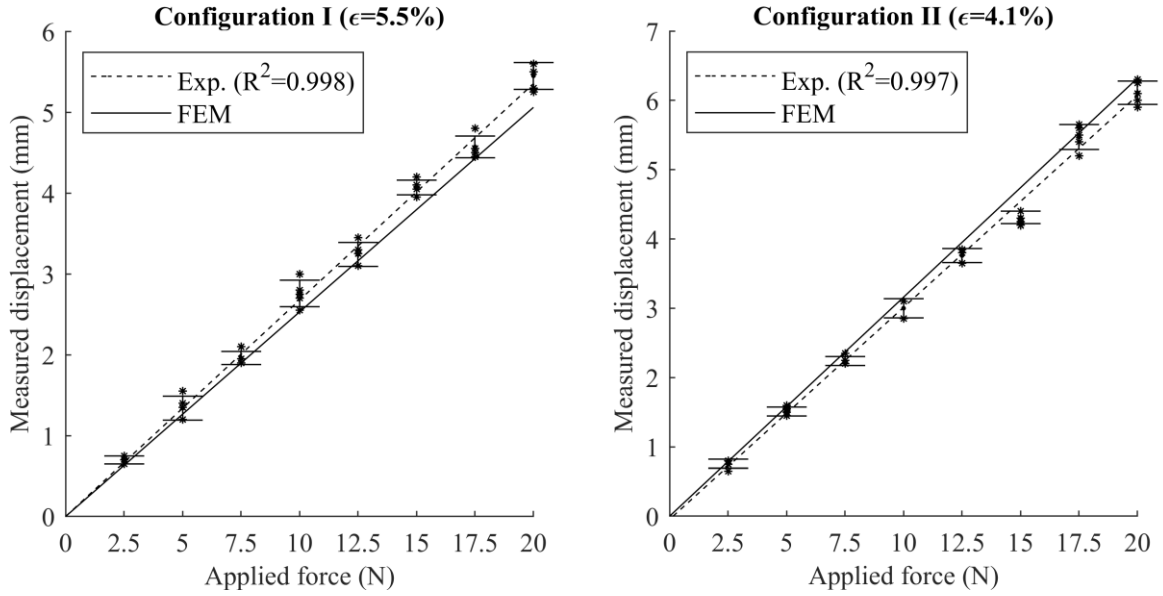

Figure 9. Experimental and FEM results comparison. Error bars: mean ± SD.

4. Conclusions

The material characteristics obtained from our tensile tests differ significantly from those stated by the manufacturer. The measured tensile strength is 15% lower than stated and the measured Young's modulus is 39% lower. This disagreement is most probably due to the unavoidably different post-curing conditions. Moreover, Formlabs followed the ASTM D 638 standard to determine tensile strength and Young's modulus [28], while in the present work the ISO 527 was adopted; therefore, different sample shapes and/or testing speeds might also partly contribute to the discrepancy in results. More importantly, Formlabs does not state the ambient temperature at which the tensile tests were performed: lower temperatures tend to increase maximum stress and Young's modulus and a difference of just a couple of degrees Celsius can be significant.

Using the actual in-house measured properties for the FEM analyses, the error between FEM and experimental results is just $\epsilon = 5.5\%$ for configuration I and $\epsilon = 4.1\%$ for configuration II. Considering the inevitable sources of variability that affect polymer testing, such errors are small, therefore these results are in very good agreement.

From a general perspective, our results confirm that, when studying the mechanical performance of SLA 3D-printed parts, it is good practice to characterize the mechanical properties of the resin using the same print settings, post-curing settings and ambient conditions as the final part. In the first stages of product development, technical datasheets are helpful to choose the right material for a determined application or to compare different materials from the same manufacturer; however, in successive phases, where a detailed knowledge of the mechanical characteristics is required, it is recommended to perform in-house tests to obtain the actual material behavior for each specific application. Moreover, it is important to consider the geometry of the designed part, which might be an obstacle to its complete polymerization. Further tests on a prototype might be necessary to confirm the predicted mechanical response. In the present study, the 3D-printed support is neither very bulky nor geometrically complex, therefore the curing process was complete throughout the part, as demonstrated by the excellent agreement between experimental and FEM results.

References

[1] Dal Maso A and Cosmi F 2019 *Materials Today: Proceedings* **12** 252-61
[2] Cha Y H, Lee K H, Ryu H J, Joo I W, Seo A, Kim D H and Kim S J 2017 *Applied bionics and biomechanics* **2017** ID9610468
[3] Goole J and Amighi K 2016 *International Journal of Pharmaceutics* **499** 376-94
[4] Jindal P, Juneja M, Siena F L, Bajaj D and Breedon P 2019 *American Journal of Orthodontics and Dentofacial Orthopedics,* **156** 694-701
[5] Rengier F, Mehndiratta A, Von Tengg-Kobligk H, Zechmann C M, Unterhinninghofen R, Kauczor H U and Giesel F L 2010 *International journal of computer assisted radiology and surgery* **5** 335-41
[6] Ryan J R, Almefty K K, Nakaji P and Frakes D H 2016 *World neurosurgery* **88** 175-81
[7] Lioufas P A, Quayle M R, Leong J C and McMenamin P G 2016 *Plastic and Reconstructive Surgery Global Open,* **4**
[8] Witowski J S, Coles-Black J, Zuzak T Z, Pędziwiatr M, Chuen J, Major P and Budzyński A 2017 *Telemedicine and e-Health* **23** 943-7
[9] Andolfi C, Plana A, Kania P, Banerjee P P and Small S 2017 *Journal of Laparoendoscopic & Advanced Surgical Techniques* **27** 512-5
[10] Clifton W, Damon A, Nottmeier E and Pichelmann M 2020 *Clinical Anatomy* **33** 124-7
[11] Cosmi F e et al 2015 *The Bone Structure Index: a study on bone quality* in *Fourth International Conference on Mechanics of Biomaterials & Tissues* Waikoloa Beach Marriott Resort, Hawaii, USA.
[12] Cosmi F 2015 *Molecular & Cellular Biomechanics* **12** 87-105
[13] Cosmi F and Nicolosi A 2018 *Materials Today: Proceedings* **5** 26667-72
[14] Melchels F P, Feijen J and Grijpma D W 2010 *Biomaterials* **31** 6121-30

[15] Nizam A, Gopal R, Naing N L, Hakim A B and Samsudin A R 2006 *Archives of Orofacial Sciences* **1** 60-6
[16] Wang J, Goyanes A, Gaisford S and Basit A W 2016 *International journal of pharmaceutics* **503** 207-12
[17] Ahn D, Kwon S and Lee S 2008 *Expression for Surface Roughness Distribution of FDM Processed Parts* in *International Conference on Smart Manufacturing Application*
[18] Nancharaiah T, Raju R and Ramachandra Raju V 2010 *International Journal of Emerging Technologies* **1** 106-11
[19] Cekic A, Begic-Hajdarevic D, Cohodar M, Muhamedagic K and Osmanlic M 2019 *Annals of DAAAM & Proceedings* **30**
[20] Phillips B T, Allder J, Bolan G, Nagle R S, Redington A, Hellebrekers T, Borden J, Pawlenko N and Licht S 2020 *Additive Manufacturing* **31**
[21] Dulieu-Barton J M and Fulton M C 2000 *Strain* **36** 81-7
[22] Quintana R, Choi J W, Puebla K and Wicker R 2010 *The International Journal of Advanced Manufacturing Technology* **46** 201-15
[23] Chantarapanich N, Puttawibul P, Sitthiseripratip K, Sucharitpwatskul S and Chantaweroad S 2013 *J. Sci. Technol.* **35** 91-8
[24] Hague R, Mansour S, Saleh N and Harris R 2004 *Journal od Material Science* **39** 2457-64
[25] Dizon J C, Espera A H, Chen Q and Advincula R C 2018 *Add Manuf* **20** 44-67
[26] Cosmi F and Dal Maso A 2020 *Materials Today: Proceedings*
[27] Salmoria G V, Ahrens C H, Fredel M, Soldi V and Pires A T 2005 *Polymer Testing* **24** 157-62
[28] Zguris Z 2016 *Formlabs Inc.*, Somerville, MA
[29] Sun Q, Rizvi G, Bellehumeur C T and Gu P 2008 *Rapid Prototyping Journal* **14** 72-80
[30] Dal Maso A and Cosmi F 2018 *Materials Today: Proceedings* **5** 26739-46
[31] Yang Y, Li L and Zhao J 2019 *Materials and Design* **162** 418-28
[32] *ISO 527: 2012 Plastics - Determination of tensile properties*
[33] Cosmi F and Dal Maso A 2019 *Proceedings of the Institution of Mechanical Engineers. Part C, Journal Mechanical Engineering Science*
[34] Khoei A R, Tabarraie A R and Gharehbaghi S A 2005 *Communications in Nonlinear Science and Numerical Simulation* **10** 253-86
[35] Formlabs 2019 *Materials Data Sheet*